


Exciton condensation in biased bilayer graphene

Harley D. Scammell^{1,2} and Oleg P. Sushkov²¹*School of Mathematical and Physical Sciences, University of Technology Sydney, Ultimo, NSW 2007, Australia*²*School of Physics, the University of New South Wales, Sydney, NSW, 2052, Australia* (Received 25 January 2023; revised 29 August 2023; accepted 5 September 2023; published 27 November 2023)

We consider suspended bilayer graphene under applied perpendicular electric bias field that is known to generate a single particle gap 2Δ and a related electric polarization \mathcal{P} . We argue that the bias also drives a quantum phase transition from band insulator to superfluid exciton condensate. The transition occurs when the exciton binding energy exceeds the band gap 2Δ . We predict the critical bias (converted to band gap), $\Delta_c \approx 60$ meV, below which the excitons condense. The critical temperature, $T_c(\Delta)$, is maximum at $\Delta \approx 25$ meV, $T_c^{\max} \approx 115$ K, decreasing significantly at smaller Δ due to thermal screening. Entering the condensate phase, the superfluid transition is accompanied by a cusp in the electric polarization $\mathcal{P}(\Delta)$ at $\Delta \rightarrow \Delta_c$, which provides a striking testable signature. Additionally, we find that the condensate prefers to form a pair density wave.

DOI: [10.1103/PhysRevResearch.5.043176](https://doi.org/10.1103/PhysRevResearch.5.043176)

I. INTRODUCTION

Excitonic condensates in two-dimensional (2D) materials promise novel superfluid [1–5] or topological [6–11] properties, and have thereby attracted considerable theoretical and experimental attention. Moreover, due to these novel transport behaviors, excitonic condensates promise a route to future technological advancements. So far, however, experimental realizations of the desired condensate have proven problematic.

Theoretically it is convenient to classify exciton condensates (also known as exciton insulators) by the nature of the corresponding interaction-driven quantum phase transition. Class I corresponds to the (semi)metal-to-exciton condensate phase transition [12–14]. In this case there are simultaneous Fermi surfaces of electrons and holes. If the Fermi surfaces are identical, an arbitrarily weak attraction between electrons and holes leads to condensation. This situation is analogous to BCS superconductivity. Class II corresponds to the band insulator-to-exciton condensate phase transition. In this case there is no Fermi surface and the interaction must exceed a critical value to generate the condensate.

Graphene layers, with their very near particle-hole symmetry, have provided a hunting ground for exciton condensation. Previous theoretical considerations include bilayer graphene (BLG), unbiased with AB stacking [15–17] or biased with AA stacking [18,19]. There have been no corresponding experimental detections of condensation.

Another set of proposals are graphene double layers [20–24] or double bilayers [25–28], separated by a dielectric. Theoretical predictions for the Berezinskii-Kosterlitz-Thouless (BKT) transition temperature for such systems vary

significantly from room temperature in Ref. [20] to 1 mK in Refs. [23,24]; the key difference arises due to the inclusion [23,24] or exclusion [20] of Coulomb screening. Experimentally, there is one recent indirect indication of possible zero-magnetic field exciton condensation in double-bilayer graphene with WSe₂ spacer [29] and also in an InAs/GaSb bilayer [30], with both scenarios belonging to Class I. On the other hand, there have been several experimental reports of exciton condensation in quantum Hall regime in strong magnetic field for double-layer graphene [31–33] or other double-layer systems [4,34,35]; such excitonic pairing occurs between different Landau levels.

Most, if not all, previous studies of exciton condensation have been aimed at class I. However, class I is necessarily a many-body problem and progress often requires uncontrolled approximations. Here, instead, we consider condensation in class II. A striking technical advantage is that we only need to consider a two-body problem. In class II the condition of exciton condensation is the equality of the exciton binding energy ϵ_b to the single-particle band gap, 2Δ . The present work is focused on biased BLG. Unbiased BLG is a semimetal, however, application of an electric bias (perpendicular electric field) opens a single-particle band gap 2Δ [36], placing it within class II. The bias is created by symmetric metallic gates above and below the plane.

A careful treatment of the screened attractive electron-hole Coulomb interaction is essential to make quantitative predictions of the binding energy and hence of the condensation transition. To this end, we account for three sources of screening: (i) screening by metallic gates placed a distance d above and below the BLG plane; (ii) dielectric screening due to a material between BLG and the gates; and (iii) BLG self-screening and retardation thereof, as captured via the random phase approximation (RPA). We find that all three sources of screening significantly influence, i.e., reduce, the condensation critical temperature. To this end, we propose idealized experimental setups to allow us to maximize the critical temperature. A key development in this work is our

Published by the American Physical Society under the terms of the [Creative Commons Attribution 4.0 International](https://creativecommons.org/licenses/by/4.0/) license. Further distribution of this work must maintain attribution to the author(s) and the published article's title, journal citation, and DOI.

treatment of the retardation of the self-screening, i.e., retardation of the screened Coulomb potential.

The key development of this work is that we are able to use reliable two-body techniques to describe excitonic bound states in a band insulator and account for environmental sources of screening; treat dynamically screening/retardation. This combination affords a reliable prediction of the critical temperature and how it may be optimized with respect to system parameters. As a corollary, our theory explains why previous experimental studies of bilayer graphene and related materials has not achieved exciton condensation. Entering the exciton condensate phase, we lose this quantitative control over the problem, and instead resort to mean-field theory. We note that the exciton condensate is a neutral superfluid, and that experimentally distinguishing between this and the band insulator phase is subtle. Using our mean-field description, we establish two key experimental signatures of the excitonic condensate.

II. METHODS

We consider biased bilayer graphene for which the low-energy single-particle Hamiltonian can be reduced to [37]

$$H_0 = \begin{pmatrix} \Delta - \mu & -\frac{p^2}{2m} \\ -\frac{p^2}{2m} & -\Delta - \mu \end{pmatrix}. \quad (1)$$

H_0 is written in terms of $\{A_1, B_2\}$ orbitals, with A, B referring to graphene sublattice and subscripts 1,2 referring to layers. Here $p_{\pm} = \tau p_x \pm i p_y$, \mathbf{p} is the in-plane momentum, $\tau = \pm 1$ the valley quantum number, $m \approx 0.032m_e$ the effective mass, and Δ is proportional to the bias electric field, $\Delta \propto E$, [38]. The chemical potential μ is set to zero (half-filling) for the rest of this work. There are corrections to (1) related to electron-hole asymmetry, trigonal warping, etc. However, influence of all these corrections on the exciton is negligible at $\Delta < 60$ meV, see Ref. [39], so here we disregard the corrections. Hence electron and hole dispersions, denoted $\omega_p^{(\pm)}$, are symmetric about $\mu = 0$, i.e., $\omega_p^{(\pm)} = \pm \omega_p$, with $\omega_p = \sqrt{\Delta^2 + p^4/(4m^2)}$. Application of the bias induces electric polarization along the field. If $a \approx 0.3$ nm is the separation between the planes and e is the electron charge, the electric dipole moment per unit area is $|e|a\mathcal{P}_{\Delta}$, with the layer polarization \mathcal{P}_{Δ} , due to the bias $\propto \Delta$, given by

$$\mathcal{P}_{\Delta} = 4 \int \frac{d^2p}{(2\pi)^2} (|\beta_p^{(-)}|^2 - |\alpha_p^{(-)}|) = \frac{2m\Delta}{\pi} \ln \frac{\Lambda}{|\Delta|}. \quad (2)$$

The factor 4 is due to the spin and valley degeneracy, $\alpha_{p,\tau}^{(-)}$ and $\beta_{p,\tau}^{(-)}$ are upper and lower components of the negative energy eigenfunction (for a given valley), and Λ is the ultraviolet energy cutoff. We confirm via a direct calculation that including the next two orbitals, i.e., $\{A_2, B_1\}$, naturally cuts off of the UV divergence; the choice $\Lambda = 0.5$ eV in (2) is consistent with the direct four-orbital calculation.

Attraction between electron and hole is due to the screened Coulomb interaction

$$V_{q,i\xi} = -\frac{2\pi e^2}{\epsilon_r q / \Upsilon_q - 2\pi e^2 \Pi(\mathbf{q}, i\xi, T)}. \quad (3)$$

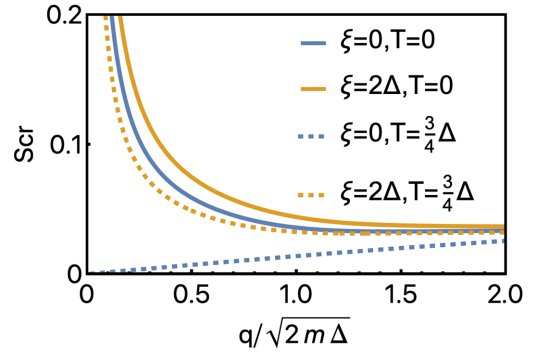


FIG. 1. Screening factor vs momentum for $\Delta = 10$ meV, $d = 1000$ nm, $\epsilon_r = 1$. The factor is presented for two imaginary frequencies, $\xi = 0$, $\xi = 2\Delta$, and for two temperatures, $T = 0$, $T = 3\Delta/4 = 87$ K.

Here \mathbf{q} is the momentum transfer, ξ is the imaginary frequency transfer, and T is temperature. Other parameters are: (i) $\Upsilon_p = \tanh(pd)$ accounts for the metallic gate screening, at a distance d above and below the BLG plane; (ii) ϵ_r is the dielectric constant of the substrate/superstrate material between BLG and gates; and (iii) $\Pi(\mathbf{q}, i\xi, T)$ is the polarization operator of BLG, with details presented in Appendix B. To demonstrate key features of (3), we introduce a screening factor, defined as the ratio of the screened interaction (3) to the bare Coulomb interaction, $-2\pi e^2/(\epsilon_r q)$. The screening factor provides a measure of the effectiveness of screening. Figure 1 demonstrates that the screening very strongly depends on frequency and on temperature. Notably, thermally excited electrons practically fully screen the static interaction, i.e. the screening factor becomes vanishingly small.

A frequency dependence of $V_{q,i\xi}$ corresponds to retardation of the interaction in the time-domain. For a weakly bound exciton in an insulator, with binding energy $\epsilon_b \ll 2\Delta$, retardation is not important [39]. However, retardation becomes essential for strongly bound excitons $\epsilon_b \sim 2\Delta$. We point out that the condition for exciton condensation, $\epsilon_b = 2\Delta$, necessarily implies strongly bound excitons and therefore retardation is important. To properly treat retardation in the exciton binding problem, one has to employ the Bethe-Salpeter equation (BSE) [40] (see Appendix D)

$$\chi_{\xi_n, \mathbf{k}} = -T \sum_m \int \frac{d^2k'}{(2\pi)^2} \frac{V_{\mathbf{k}-\mathbf{k}', i(\xi_n - \xi_m)} Z_{\mathbf{k}, \mathbf{k}'}^{\tau', \tau}}{(E/2 - \omega_{\mathbf{k}})^2 + \xi_n^2} \chi_{\xi_m, \mathbf{k}'}, \quad (4)$$

written in terms of the amputated two-particle Green's function $\chi_{\xi_n, \mathbf{k}}$. Here $E = 2\Delta - \epsilon_b$, $\xi_n = (2n + 1)\pi T$ and $Z_{\mathbf{k}, \mathbf{k}'}^{\tau', \tau} = \langle \psi_{\mathbf{k}, \tau}^{(-)} | \psi_{\mathbf{k}', \tau'}^{(-)} \rangle \langle \psi_{\mathbf{k}', \tau}^{(+)} | \psi_{\mathbf{k}, \tau}^{(+)} \rangle$ is the vertex form factor, with $\psi_{\mathbf{k}, \tau}^{(\pm)}$ denoting the single-particle wave functions for conduction and valence bands of (1), see also Appendix C. The total momentum of the electron and hole is encoded in the valley indices, and is either zero for $\tau = \tau'$ (intravalley pairing) or nonzero for $\tau = -\tau'$ (intervalley pairing), as depicted in Fig. 2. The form factors do not distinguish spin, yet they weakly distinguish between intra- and intervalley pairing; the implications for the condensate phase is discussed later. The interaction has an $SU(2) \times SU(2)$ spin symmetry;

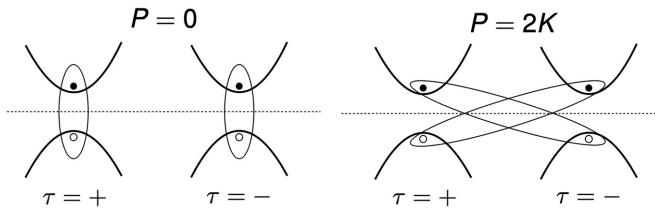


FIG. 2. Inter- and intravalley excitons: intravalley have zero total momentum $P = \mathbf{0}$, while intervalley have $P = 2\mathbf{K}$, with \mathbf{K} the valley momentum.

correspondingly, the exciton bound state has an $SO(4)$ spin symmetry relating the spin-singlet and -triplet configurations.

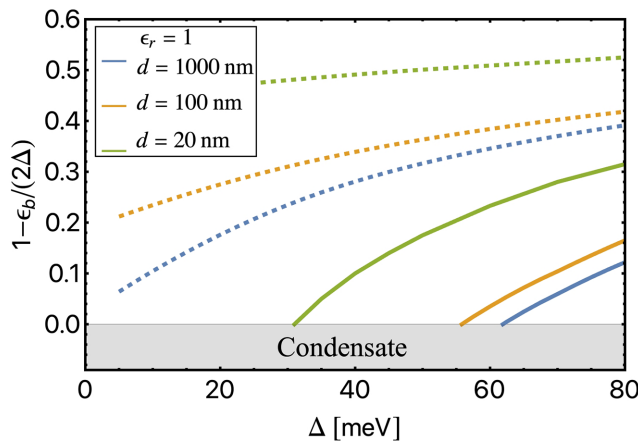
We pause to mention that under an instantaneous interaction, $V_{k-k'}$, e.g., as obtained by ignoring the frequency dependence of screening, the exciton can be described by a wave function that obeys the Lippmann-Schwinger equation (LSE),

$$(E_0 - 2\omega_k)\Psi_k = \int \frac{d^2k'}{(2\pi)^2} V_{k-k'} Z_{k,k'}^{\tau',\tau} \tanh\left(\frac{\omega_{k'}}{2T}\right) \Psi_{k'}. \quad (5)$$

LSE is a linear eigenvalue problem and can be easily solved to find the eigenenergy E_0 and eigenfunction Ψ_k ; solution of (5) shows that the Lippmann-Schwinger wave function Ψ_k is well localized in the momentum space, $k \lesssim \sqrt{2m\Delta}$. This corresponds to the exciton spatial size $r \sim 1/\sqrt{2m\Delta}$. We see a hint that the wave-function approach is problematic at $\Delta \rightarrow 0$. We denote the binding energy computed from LSE as $\epsilon_b^0 = 2\Delta - E_0$.

III. PHASE DIAGRAM

Via direct computation of Eq. (4), the intervalley s -wave exciton is found to have the lowest energy for $\Delta > 0$; we henceforth specialize to this state. Let us start from $T = 0$. Figure 3(a) shows the exciton binding energy vs the gap parameter Δ for $\epsilon_r = 1$ and three values of distance to the gate $d = \{20, 100, 1000\}$ nm; the solid and dashed lines are computed from the BSE (4) and LSE (5), respectively, whereby



only the BSE includes retardation effects. First, we see that retardation significantly influences the binding energy; one could think of retardation of the screened potential acting as an effective dynamic boson mode, which is enhancing the binding of electrons and holes. Second, the plot marks a condensation region, whereby $\epsilon_b \geq 2\Delta$. At $\epsilon_r = 1$, condensation occurs for gates placed beyond a critical distance $d > d_c \approx 10\text{--}15$ nm. In particular, for $d = \{20, 100, 1000\}$ nm the quantum critical point is $\Delta_c = \{31, 55, 62\}$ meV. Considering instead hBN encapsulation, such that $\epsilon_r = 3.9$, and taking $d = 100$ nm, the critical point is reduced to $\Delta_c = 3$ meV. These results highlight the strong influence of gate and dielectric screening on the excitonic binding energy and condensation transition.

To establish the phase boundary of Fig. 3(b), we solve $\epsilon_b(T_c) = 2\Delta$. We note that for $\Delta < \Delta_c$, the two-particle problem makes sense only at or above the critical temperature, where T_c is understood to be a BKT transition temperature. For $\epsilon_r = 1$ and $d = \{100, 1000\}$ nm maximum critical temperatures are significant, $T_c \approx \{100, 115\}$ K, respectively. For $\epsilon_r = 3.9$, $d = 100$ nm the superfluid dome is comparatively small. Figure 3(b) shows that as $\Delta \rightarrow 0$, the $T_c(\Delta)$ is rapidly decreasing. However, we stress that we do not propagate the BSE technique down to exactly $\Delta = 0$; here the system becomes semimetallic and the two-body technique employed here becomes prohibitively expensive numerically. Physically, the strong suppression of T_c at small band gap Δ is due to the enhanced thermal excitation to the conduction band; the thermally excited states act as a source of metallic screening, and thereby have a significant affect on the Coulomb attraction. This feature, i.e., strongly enhanced screening, makes this problem highly non-BCS; BCS provides a simple relation between $T = 0$ order parameter and T_c , which derives from the Pauli blocking factor (i.e., thermal occupation factors). In our case, we have both (thermal) Pauli blocking as well as thermal screening of the interaction. We find that the thermal screening plays the dominant role in melting the order, and thus we do not recover the standard BCS relation.

Finally, we mention that within the BSE two-body formalism we arrive at the following critical scaling of T_c near

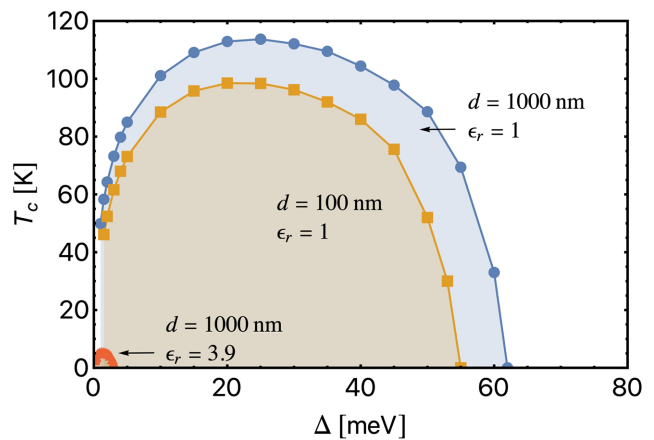


FIG. 3. (a) Exciton binding energy at $T = 0$ and three values of distance to gates, $d = 20, 100, 1000$ nm vs the band gap, at $\epsilon_r = 1$. Dashed lines correspond to LSE and solid lines to BSE. (b) Superfluid domes, for the following sets of parameters: $\{\epsilon_r = 1, d = 1000\}$ nm, $\{\epsilon_r = 1, d = 100\}$ nm, $\{\epsilon_r = 3.9, d = 1000\}$ nm. Points represent T_c versus the band gap parameter Δ , as computed from the BSE (4).

$\Delta \rightarrow \Delta_c^-$ (see Appendix F),

$$T_c(\Delta) \sim \Delta_c / \ln \left(\frac{g\Delta_c}{\Delta_c - \Delta} \right), \quad (6)$$

where g is a dimensionless combination of the interaction strength and density of states, as well as other dimensionless numerical factors that we do not evaluate.

IV. CONDENSATE PHASE

Entering the condensate phase we can no longer apply two-body techniques, and therefore do not expect to make quantitative predictions. Even so, the results below provide crucial predictions for future experimental tests of the exciton condensate. The discussion from here on will be based on a mean-field Hamiltonian, $H_{\text{MF}} = \sum_{p,\tau,s} c_{p,\tau,s}^\dagger \omega_p c_{p,\tau,s} + v_{p,\tau,s}^\dagger (-\omega_p) v_{p,\tau,s} + \sum_{p,\tau,\tau',s,s'} c_{p,\tau,s}^\dagger \Phi(p)_{\tau,\tau',s,s'} v_{p,\tau',s'} + \text{H.c.}$, with $c_{p,\tau,s}^\dagger$ ($v_{p,\tau,s}^\dagger$) the creation operators for conduction (valence) electrons, and with $\Phi(p)_{\tau,\tau',s,s'}$ the order parameter. Explicitly for the s -wave intervalley excitonic condensate, it takes the form

$$\Phi(p)_{\tau,\tau',s,s'} = \Phi_0(p) (\tau_x)_{\tau,\tau'} e^{i\frac{(\tau-\tau')}{2}\phi} (d_\mu s_\mu i s_y)_{s,s'}, \quad (7)$$

where $\Phi_0(p)$ is the amplitude; ϕ an arbitrary phase encoding the phase difference between the two distinct intervalley states, i.e., those with valley indices $(\tau, \tau') = (+-)$ and $(-+)$; τ_x is a Pauli matrix acting on valley indices; s_μ are Pauli spin matrices; and d_μ are the components of a unit four-vector, with $\mu = 0$ corresponding to a spin singlet and $\mu = 1, 2, 3$ to the components of the spin triplet. There is an SO(4) degeneracy of this spin ordering vector (d_μ).

We pause to note that a spontaneous symmetry breaking in unbiased bilayer graphene has been considered [15]. Specifically, that work predicts a spontaneous ferroelectric polarization perpendicular to the plane, breaking a \mathbb{Z}_2 layer symmetry. By contrast, in the present work the applied electric bias explicitly breaks the \mathbb{Z}_2 symmetry and drives a single-particle band gap (2Δ). Our key prediction is the spontaneous breakdown of a U(1) symmetry, and hence the onset of superfluidity. We stress that the superfluid order parameter [Eq. (7)] is not a ferroelectric; it does not couple linearly to an external electric field. However, it does influence the layer polarization in a measurable way and this opens a unique way to detect the superfluid quantum phase transition. We discuss these details next.

Within the ordered phase $\Delta < \Delta_c$, and at $T = 0$, we appeal to the BCS/Eliashberg gap equation to estimate $\Phi_0(p)$ [for simplicity we, for now, ignore the momentum dependence, such that $\Phi_0(p) = \Phi_0$]. Near the critical point $\Delta \rightarrow \Delta_c$, and to logarithmic accuracy, the gap equation gives $1 = g' \ln(\Lambda'/\sqrt{\Delta^2 + |\Phi_0|^2})$ or $|\Phi_0| = \text{Re}\sqrt{\Delta_c^2 - \Delta^2}$. Here $\Delta_c = \Lambda' e^{-1/g'}$, $g' \sim g$ is a dimensionless combination of the interaction and density of states and $\Lambda' \sim \Lambda$ is a UV cutoff.

The natural, measurable quantity of the system is not Φ_0 , but instead the layer polarization. In the absence of excitonic order, $\Phi_0 = 0$, the polarization is \mathcal{P}_Δ of Eq. (2). polarization results from the valence electrons belonging predominantly to, say, the bottom layer. Since $\Phi_0 \neq 0$ ultimately corresponds to removing valence electrons (bottom

layer) and enhancing conduction electrons (top layer), one expects $\Phi_0 \neq 0$ to reduce the ground-state polarization. The polarization in the condensate phase is then simply $\mathcal{P}_{\Delta,\Phi_0} = \frac{2m\Delta}{\pi} \ln(\Lambda/\sqrt{\Delta^2 + |\Phi_0|^2})$. We see that $\Phi_0 \neq 0$ indeed reduces the layer polarization, with leading correction quadratic in Φ_0 . Further, we appeal to the gap equation solution to arrive a key prediction,

$$\mathcal{P}_{\Delta,\Phi_0} - \mathcal{P}_\Delta = -\frac{m|\Phi_0|^2}{\pi\Delta} \xrightarrow{\Delta \rightarrow \Delta_c^-} -\frac{2m(\Delta_c - \Delta)}{\pi}. \quad (8)$$

This expression shows that there is a linear in Δ (and hence in external electric field E) reduction of the layer polarization in the vicinity of the critical point. We anticipate the polarization being readily measured via quantum capacitance, see, e.g., Refs. [30,41,42], which would provide a direct experimental test of the exciton condensation transition.

Finally, we turn to the in-plane real-space structure of the condensate. The intervalley ordering [Eq. (7)] implies that, in real space, the condensate exhibits a pair density wave pattern, denoting $\tilde{\Phi}_{s,s'}(\mathbf{r}, \mathbf{r}') = \tilde{\Phi}(\mathbf{r}, \mathbf{r}') (d_\mu s_\mu i s_y)_{s,s'}$,

$$\tilde{\Phi}(\mathbf{r}, \mathbf{r}') = \tilde{\Phi}_0(\mathbf{r} - \mathbf{r}') \cos(\mathbf{K} \cdot (\mathbf{r} + \mathbf{r}') + \phi) \quad (9)$$

with $\tilde{\Phi}_0(\mathbf{r} - \mathbf{r}')$ a complex amplitude (derived in the Appendix G). Fluctuations of ϕ correspond to gapless sliding modes of the pair density wave. The pair density wave is spatially modulated with a periodicity of three unit cells. It is worth noting that under a particle-hole transformation, the excitonic pair can be mapped to the superconducting Cooper pair, as shown in, e.g., Ref. [43]. Building on this insight, it is natural to compare the phenomenology of the excitonic and superconducting pair density waves. A detailed analysis of the analogous superconducting density wave pattern has already been conducted in Ref. [44], and this pattern has been associated with higher-order topology in Refs. [45,46]. However, the question of whether the excitonic pair density wave in Eq. (9) exhibits higher topology remains for future work.

V. DISCUSSION

We presented a description of excitonic bound states in biased BLG and their subsequent condensation, using two-body techniques. This is in contrast to exciton formation and condensation from a semimetallic ground state, which require many-body techniques that often lead to uncontrolled approximations. We studied suspended biased BLG with gates at $d > d_c \approx 10\text{--}15$ nm and found that excitons condense for $\Delta < \Delta_c$, as shown in Fig. 3(a). Our primary theoretical finding is that at distances $d = 100$ nm (1000 nm), the maximum critical temperature is predicted to be 100 K (115 K), and is optimized at nonzero bias, as shown in Fig. 3(b).

Regarding previous experiments on biased bilayer graphene, we discuss Refs. [47–49]. Reference [49] uses parameters $d \approx 20$ nm and $\epsilon = 3.9$ (hBN encapsulation), and examines $\Delta \gtrsim 20$ meV. Consistent with our predictions (Fig. 3), they do not observe exciton condensation. On the other hand, Refs. [47,48] use $d \approx 20$ nm, $\epsilon = 1$ (suspended), and probe a range of Δ down to $\Delta = 0$. Based on our modeling, exciton condensation is expected, and indeed both Refs. [47,48] report a Coulomb-driven band gap opening at $\Delta = 0$; we suggest that this is

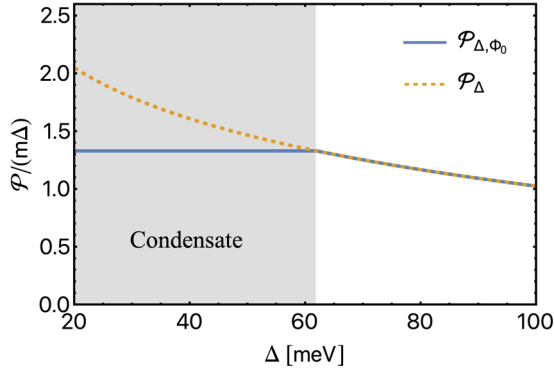


FIG. 4. Dimensionless layer polarization, as a function of band gap parameter Δ , with and without the condensate, corresponding to $\mathcal{P}_{\Delta,\Phi}$ and \mathcal{P}_{Δ} [Eq. (2)], respectively. Here we use the meanfield expression $|\Phi_0| = \text{Re}\sqrt{\Delta_c^2 - \Delta^2}$, at $T = 0$, with $\Delta_c = 62$ meV corresponding to system parameters $\epsilon_r = 1$, $d = 1000$ nm. Due to the onset of the condensate Φ , a cusp is seen in reduced layer polarization, $\mathcal{P}_{\Delta,\Phi}/(m\Delta)$, at the critical point Δ_c .

consistent with exciton condensation. Therefore, it is crucial to perform further studies, ideally at $d = 100$ nm, to examine the possibility of exciton condensation in suspended bilayer graphene. The question is, how best to detect the condensate?

Our work proposes a solution. Although our two-body techniques become less accurate upon entering the BEC phase, we were able to establish several qualitative features of the condensate. Distinguishing between the excitonic condensate/insulator and the band insulator experimentally is challenging. However, we found that excitons influence the macroscopic dipole moment [cf. (8)], and proposed a smoking-gun test for exciton condensation: quantum capacitance measurements of the dipole moment as a function of the bias field, which tunes the band insulator to exciton condensate phase transition (cf. Fig. 4). We hope that our findings entice direct experimental searches for the excitonic condensate in biased bilayer graphene, and future theoretical work may consider other candidate materials using the two-body approach applied here.

ACKNOWLEDGMENTS

We thank D. Efimkon, A. Hamilton, M. Zhitomirsky, and J. Schmalian for enlightening conversations. We acknowledge funding support from the Australian Research Council Centre of Excellence in Future Low-Energy Electronics Technology (FLEET) (CE170100039).

APPENDIX A: HAMILTONIAN AND WAVE FUNCTIONS

The Hamiltonian and wave functions are (in zero field)

$$H_{\tau} = -\frac{(\tau p_x \mp i p_y)^2}{2m} \sigma_{\pm} + \Delta \sigma_z$$

$$|\psi_{p,\tau}^{(+)}\rangle = \frac{1}{\sqrt{\frac{(\epsilon_p - \Delta)^2}{p^4/(4m^2)} + 1}} \begin{pmatrix} -1 \\ \frac{\epsilon_p - \Delta}{p^2/(2m)} e^{2i\tau\theta_p} \end{pmatrix},$$

$$|\psi_{p,\tau}^{(-)}\rangle = \mathcal{P}|\psi_{p,\tau}^{(+)}\rangle = \frac{1}{\sqrt{\frac{(\epsilon_p - \Delta)^2}{p^4/(4m^2)} + 1}} \begin{pmatrix} \frac{\epsilon_p - \Delta}{p^2/(2m)} e^{-2i\tau\theta_p} \\ 1 \end{pmatrix},$$

$$\mathcal{P} = i\sigma_y \mathcal{C}. \quad (\text{A1})$$

Here \mathcal{C} enacts complex conjugation and the operator \mathcal{P} generates the particle-hole transformation, which is an anti-commuting symmetry of this Hamiltonian. Defining ψ_- in this way correctly generates the phase/winding factors.

APPENDIX B: POLARIZATION OPERATOR

The expression for the polarization generically takes the form,

$$\Pi(\mathbf{q}, i\xi, T) = 4 \sum_{\mu, \nu = \pm} \int \frac{d^2 p}{(2\pi)^2} \frac{(f_{\epsilon_p^{\mu}} - f_{\epsilon_{p+q}^{\nu}})}{i\xi + \epsilon_p^{\mu} - \epsilon_{p+q}^{\nu}} F_{p,p+q}^{\mu\nu}. \quad (\text{B1})$$

Here the form factors are $F_{p,p+q}^{\mu\nu} = |\langle \psi_{p+q,\tau}^{(\mu)} | \psi_{p,\tau}^{(\nu)} \rangle|^2$, with $\mu, \nu = \pm$. Using that $-\epsilon_p^- = \epsilon_p^+ \equiv \epsilon_p$ and $F_{p,p+q}^{--} = F_{p,p+q}^{++}$, $F_{p,p+q}^{-+} = F_{p,p+q}^{+-}$, we get

$$\Pi(\mathbf{q}, i\xi, T) = 8 \int \frac{d^2 p}{(2\pi)^2} \left[\frac{(\epsilon_p - \epsilon_{p+q})(f_{\epsilon_p} - f_{\epsilon_{p+q}})}{\xi^2 + (\epsilon_p - \epsilon_{p+q})^2} F_{p,p+q}^{++} \right. \\ \left. + \frac{(\epsilon_p + \epsilon_{p+q})(f_{\epsilon_p} + f_{\epsilon_{p+q}} - 1)}{\xi^2 + (\epsilon_p + \epsilon_{p+q})^2} F_{p,p+q}^{+-} \right]. \quad (\text{B2})$$

APPENDIX C: VERTEX FORM FACTORS

The Coulomb interaction is taken to be

$$H_{\text{int}} = \sum_{p_1, p_2, p_3} \sum_{\tau, \tau'} V(\mathbf{p}_2 - \mathbf{p}_1) \Psi_{p_1, \tau}^{\dagger} \Psi_{p_2, \tau'}^{\dagger} \Psi_{p_3, \tau'} \Psi_{p_1 + p_2 - p_3, \tau}, \quad (\text{C1})$$

which neglects valley exchange. We transform to band basis,

$$\Psi_{p,\tau} = \mathcal{U}_{p,\tau} \begin{pmatrix} c_{p,\tau} \\ v_{p,\tau} \end{pmatrix}, \quad \mathcal{U}_{p,\tau} = (|\psi_{p,\tau}^{(+)}\rangle, |\psi_{p,\tau}^{(-)}\rangle),$$

with $c_{p,\tau}$ and $v_{p,\tau}$ the destruction operators for conduction and valence electrons. Restricting consideration to the exciton channel, denoted H_{int}^X , the interaction becomes,

$$H_{\text{int}}^X = \sum_{p_1, p_2} \sum_{\tau, \tau'} V(\mathbf{p}_2 - \mathbf{p}_1) c_{p_1, \tau}^{\dagger} c_{p_2, \tau} v_{p_2, \tau'}^{\dagger} v_{p_1, \tau'} \\ \times \langle \psi_{p_2, \tau'}^{(-)} | \psi_{p_1, \tau'}^{(-)} \rangle \langle \psi_{p_1, \tau}^{(+)} | \psi_{p_2, \tau}^{(+)} \rangle. \quad (\text{C2})$$

In the main text we denote the form factor $Z_{p_1, p_2}^{\tau', \tau} = \langle \psi_{p_2, \tau'}^{(-)} | \psi_{p_1, \tau'}^{(-)} \rangle \langle \psi_{p_1, \tau}^{(+)} | \psi_{p_2, \tau}^{(+)} \rangle$.

APPENDIX D: NUMERICAL BSE SOLUTION

In this Appendix we describe the numerical method employed to solve BSE. For ease of notation, we introduce

variables

$$\begin{aligned} \mathcal{X}_{\xi,p} &= \sqrt{a_p^2 + \xi^2} \chi_{\xi,p} \\ \mathcal{V}_{p,k}(\xi - \lambda) &= \frac{V_{p,k}(\xi - \lambda) Z_{p,k}}{\sqrt{(a_p^2 + \xi^2)(a_k^2 + \lambda^2)}}, \end{aligned} \quad (\text{D1})$$

with $a_p = -E/2 + \epsilon_p$, such that the BSE more compactly reads,

$$\mathcal{X}_{\xi,p} = - \int \mathcal{V}_{p,k}(\xi - \lambda) \mathcal{X}_{\lambda,k} D_\lambda D_k. \quad (\text{D2})$$

To solve Eq.(D2), we first fix the energy E , and introduce a new variable R , such that

$$R \mathcal{X}_{\xi,p} = - \int \mathcal{V}_{p,k}(\xi - \lambda) \mathcal{X}_{\lambda,k} D_\lambda D_k. \quad (\text{D3})$$

Here, solving for R is a standard eigenvalue problem and can be efficiently performed numerically. Of the solutions, we keep the maximal eigenvalue R_{\max} . Next, we repeat this process for a range of E ; the solution to the original BSE (D2) is found when E satisfies $R_{\max}(E) = 1$.

APPENDIX E: NON-HERMITICITY OF BSE

The BS equation is written,

$$\chi_{\xi_n,k} = -T \sum_m \int \frac{d^2 k'}{(2\pi)^2} \frac{V_{k-k',i(\xi_n - \xi_m)} Z_{k,k'}^{\tau',\tau}}{(E/2 - \omega_k)^2 + \xi_n^2} \chi_{\xi_m,k'}. \quad (\text{E1})$$

Treating each $\{\xi_n, \mathbf{k}\}$ as a matrix index, then the BS can be solved as an eigenvalue problem, i.e.,

$$\bar{\chi} = -\Gamma W \bar{\chi}. \quad (\text{E2})$$

Here $\Gamma = VZ$ is Hermitian, however the combination ΓW is non-Hermitian and therefore the eigenvalues are not guaranteed to be real. However, there exists a transformation,

$$\begin{aligned} \bar{\chi} &= -\Gamma W^{\frac{1}{2}} (W^{\frac{1}{2}} \bar{\chi}) \\ W^{-\frac{1}{2}} \bar{\chi}' &= -\Gamma W^{\frac{1}{2}} \bar{\chi}' \\ \bar{\chi}' &= -W^{\frac{1}{2}} \Gamma W^{\frac{1}{2}} \bar{\chi}'. \end{aligned} \quad (\text{E3})$$

If $W^{\frac{1}{2}}$ is strictly real, then matrix on the right-hand side, i.e., $W^{\frac{1}{2}} \Gamma W^{\frac{1}{2}}$, is Hermitian. For the case in question, W is both diagonal and positive definite, i.e., since componentwise it is written

$$W_{\xi_n,k;\xi'_n,k'} = \delta_{\xi_n,k;\xi'_n,k'} \frac{1}{(E/2 - \omega_k)^2 + \xi_n^2}, \quad (\text{E4})$$

and therefore $W^{\frac{1}{2}}$ is strictly real. We also note that $\xi_n^2 = [(2n+1)\pi T]^2 > 0$, which prevents this matrix from being singular.

Finally, since our initial matrix (here denoted $M_1 \equiv \Gamma W$) and the transformed matrix (here denoted $M_2 \equiv W^{\frac{1}{2}} \Gamma W^{\frac{1}{2}}$) are related by a similarity transformation, i.e.,

$$M_1 = (W^{\frac{1}{2}})^{-1} M_2 W^{\frac{1}{2}}, \quad (\text{E5})$$

then M_1 and M_2 have the same eigenvalues and, since M_2 is Hermitian, these eigenvalues are guaranteed to be real.

APPENDIX F: CRITICAL TEMPERATURE SCALING

Setting $E = 0$, the $T = 0$ the Lippmann-Schwinger equation gives the condition for Δ_c

$$2\sqrt{\frac{p^4}{4m^2} + \Delta_c^2} \Psi_p = \int \frac{d^2 p'}{(2\pi)^2} V_{p,p'}^0 \Psi_{p'}. \quad (\text{F1})$$

At $T > 0$, the condition $E = 0$ requires $\Delta < \Delta_c$, and is given by

$$2\sqrt{\frac{p^4}{4m^2} + \Delta_c^2} \Psi_p = \int \frac{d^2 p'}{(2\pi)^2} [V_{p,p'}^0 + \delta V_{p,p'} e^{-\frac{\Delta}{T}}] \Psi_{p'}. \quad (\text{F2})$$

Using that the characteristic momentum is $p = \sqrt{2m\Delta}$, we combine these two equations as

$$\begin{aligned} \Delta_c &= v_0, \quad \Delta = (v_0 - v_1 e^{-\frac{\Delta}{T_c}}), \\ (\Delta_c - \Delta) &= v_1 e^{-\frac{\Delta}{T_c}}, \rightarrow T_c = \Delta / \ln\left(\frac{v_1}{\Delta_c - \Delta}\right). \end{aligned} \quad (\text{F3})$$

APPENDIX G: REAL-SPACE ORDER PARAMETER

In this Appendix we derive the effective lattice model for the dominant excitonic order parameter. Introducing the real-space creation operators for the conduction and valence bands via,

$$\begin{aligned} c_{p,\tau,s}^\dagger &= \sum_{\mathbf{r}} \phi_{p,\tau}^{(+)}(\mathbf{r}) \tilde{c}_{\mathbf{r},s}^\dagger, \\ v_{p,\tau,s}^\dagger &= \sum_{\mathbf{r}} \phi_{p,\tau}^{(-)}(\mathbf{r}) \tilde{v}_{\mathbf{r},s}^\dagger. \end{aligned} \quad (\text{G1})$$

With \mathbf{r} spanning the real-space lattice sites, and comprising two sublattices, $\sigma = A_1, B_2$, and $\{a(\mathbf{r} \in A) = 1, a(\mathbf{r} \in B) = 0\}$ and $\{b(\mathbf{r} \in A) = 0, b(\mathbf{r} \in B) = 1\}$. Here,

$$\begin{aligned} \phi_{p,\tau}^{(+)}(\mathbf{r}) &= e^{i(p+\tau K)} (\alpha_{\tau,k}^{(+)} a(\mathbf{r}) + \beta_{\tau,k}^{(+)} b(\mathbf{r})), \\ \phi_{p,\tau}^{(-)}(\mathbf{r}) &= e^{i(p+\tau K)} (\alpha_{\tau,k}^{(-)} a(\mathbf{r}) + \beta_{\tau,k}^{(-)} b(\mathbf{r})), \end{aligned} \quad (\text{G2})$$

with definitions,

$$\begin{aligned} \alpha_{\tau,p}^{(+)} &= -\cos \gamma_p = \frac{-1}{\sqrt{\frac{(\epsilon_p - \Delta)^2}{p^4/(4m^2)} + 1}}, \\ \beta_{\tau,p}^{(+)} &= \sin \gamma_p e^{2i\tau\theta_p} = \frac{\epsilon_p - \Delta}{p^2/(2m)} \frac{e^{2i\tau\theta_p}}{\sqrt{\frac{(\epsilon_p - \Delta)^2}{p^4/(4m^2)} + 1}}, \\ \alpha_{\tau,p}^{(-)} &= \sin \gamma_p e^{-2i\tau\theta_p} = \frac{\epsilon_p - \Delta}{p^2/(2m)} \frac{e^{-2i\tau\theta_p}}{\sqrt{\frac{(\epsilon_p - \Delta)^2}{p^4/(4m^2)} + 1}}, \\ \beta_{\tau,p}^{(-)} &= \cos \gamma_p = \frac{1}{\sqrt{\frac{(\epsilon_p - \Delta)^2}{p^4/(4m^2)} + 1}}. \end{aligned} \quad (\text{G3})$$

The mean-field Hamiltonian becomes,

$$\begin{aligned} H_\Phi &= \sum_{p,\tau,\tau',s,s'} c_{p,\tau,s}^\dagger \Phi(p)_{\tau,\tau',s,s'} v_{p,\tau',s'} + \text{H.c.} \\ &= \sum_{p,\tau,\tau',s,s'} \sum_{\mathbf{r},\mathbf{r}'} \phi_{p,\tau}^{(+)}(\mathbf{r}) (\phi_{p,\tau'}^{(-)})^*(\mathbf{r}') \Phi(p)_{\tau,\tau',s,s'} \tilde{c}_{\mathbf{r},s}^\dagger \tilde{v}_{\mathbf{r}',s'} \\ &\quad + \text{H.c.} \end{aligned} \quad (\text{G4})$$

We consider intervalley pairing in the s -wave channel and with arbitrary spin ordering (singlet or triplet). There is both a symmetric and an antisymmetric combination of the valleys,

$$\Phi(p)_{\tau,\tau',s,s'} = \begin{cases} \Phi_0(p)(\tau_x)_{\tau,\tau'}(d_\mu s_\mu)_{s,s'} \\ \Phi_0(p)(i\tau_y)_{\tau,\tau'}(d_\mu s_\mu)_{s,s'}. \end{cases} \quad (\text{G5})$$

In fact, there is a U(1) rotational symmetry that connects these distinct valley structures, we more compactly write

$$\Phi(p)_{\tau,\tau',s,s'} = \Phi_0(p)(\tau_x)_{\tau,\tau'} e^{i\frac{(\tau-\tau')\phi}{2}} (d_\mu s_\mu)_{s,s'}. \quad (\text{G6})$$

Let us consider the case that $\mathbf{r} \in A$ and $\mathbf{r}' \in B$,

$$\begin{aligned} H_\Phi^{AB} &= \sum_{p,\tau,s,s'} \sum_{\mathbf{r} \in A, \mathbf{r}' \in B} (e^{i(p+\tau\mathbf{K})\cdot\mathbf{r}} \alpha_{\tau,p}^{(+)} a(\mathbf{r})) (e^{-i(p-\tau\mathbf{K})\cdot\mathbf{r}'} \beta_{-\tau,p}^{(-)} b(\mathbf{r}')) \Phi_0(p) e^{i\tau\phi} \tilde{c}_{r,s}^\dagger \tilde{v}_{r',s'} (d_\mu s_\mu)_{s,s'} + \text{H.c.} \\ &= \sum_{p,\tau,s,s'} \sum_{\mathbf{r} \in A, \mathbf{r}' \in B} [e^{i\mathbf{p}\cdot(\mathbf{r}-\mathbf{r}')} e^{i\tau\mathbf{K}\cdot(\mathbf{r}+\mathbf{r}')} \alpha_{\tau,p}^{(+)} \beta_{-\tau,p}^{(-)} \Phi_0(p) e^{i\tau\phi}] \tilde{c}_{r,s}^\dagger \tilde{v}_{r',s'} (d_\mu s_\mu)_{s,s'} + \text{H.c.}, \\ &= \sum_{\mathbf{r} \in A, \mathbf{r}' \in B} \sum_p [2e^{i\mathbf{p}\cdot(\mathbf{r}-\mathbf{r}')} (-\cos^2 \gamma_p) \Phi_0(p)] [\cos(\mathbf{K} \cdot (\mathbf{r} + \mathbf{r}') + \phi)] \sum_{s,s'} \tilde{c}_{r,s}^\dagger \tilde{v}_{r',s'} (d_\mu s_\mu)_{s,s'} + \text{H.c.}, \\ &= \sum_{\mathbf{r} \in A, \mathbf{r}' \in B} \Gamma^{AB}(\mathbf{r} - \mathbf{r}') [\cos(\mathbf{K} \cdot (\mathbf{r} + \mathbf{r}') + \phi)] \sum_{s,s'} \tilde{c}_{r,s}^\dagger \tilde{v}_{r',s'} (d_\mu s_\mu)_{s,s'} + \text{H.c.} \end{aligned} \quad (\text{G7})$$

We have defined the function,

$$\Gamma^{AB}(\mathbf{r} - \mathbf{r}') \equiv \sum_p [2e^{i\mathbf{p}\cdot(\mathbf{r}-\mathbf{r}')} (-\cos^2 \gamma_p) \Phi_0(p)], \quad (\text{G8})$$

which determines the real-space amplitude and can be directly evaluated numerically.

Performing the same procedure for all combinations of \mathbf{r}, \mathbf{r}' in $\{A_1, B_2\}$, we arrive at the expression,

$$H_\Phi = \sum_{\mathbf{r}, \mathbf{r}'} \Gamma(\mathbf{r} - \mathbf{r}') [\cos(\mathbf{K} \cdot (\mathbf{r} + \mathbf{r}') + \phi)] \sum_{s,s'} \tilde{c}_{r,s}^\dagger \tilde{v}_{r',s'} (d_\mu s_\mu)_{s,s'} + \text{H.c.}, \quad (\text{G9})$$

with amplitude function given by,

$$\Gamma(\mathbf{r} - \mathbf{r}') = \begin{cases} \Gamma^{AA}(\mathbf{r} - \mathbf{r}') = \sum_p [2e^{i\mathbf{p}\cdot(\mathbf{r}-\mathbf{r}')} (-\cos \gamma_p \sin \gamma_p e^{\pm 2i\tau\theta_p}) \Phi_0(p)], \text{ for } \{\mathbf{r} \in A_1, \mathbf{r}' \in A_1\} \\ \Gamma^{BB}(\mathbf{r} - \mathbf{r}') = \sum_p [2e^{i\mathbf{p}\cdot(\mathbf{r}-\mathbf{r}')} (\cos \gamma_p \sin \gamma_p e^{\pm 2i\tau\theta_p}) \Phi_0(p)], \text{ for } \{\mathbf{r} \in B_2, \mathbf{r}' \in B_2\} \\ \Gamma^{AB}(\mathbf{r} - \mathbf{r}') = \sum_p [2e^{i\mathbf{p}\cdot(\mathbf{r}-\mathbf{r}')} (-\cos^2 \gamma_p) \Phi_0(p)], \text{ for } \{\mathbf{r} \in A_1, \mathbf{r}' \in B_2\} \\ \Gamma^{BA}(\mathbf{r} - \mathbf{r}') = \sum_p [2e^{i\mathbf{p}\cdot(\mathbf{r}-\mathbf{r}')} (\sin^2 \gamma_p e^{\pm 4i\theta_p}) \Phi_0(p)], \text{ for } \{\mathbf{r} \in B_2, \mathbf{r}' \in A_1\}. \end{cases} \quad (\text{G10})$$

-
- [1] Yu. E. Lozovik and V. I. Yudson, Feasibility of superfluidity of paired spatially separated electrons and holes: A new superconductivity mechanism, *Pis'ma Zh. Eksp. Teor. Fiz.* **22**, 556 (1975) [*JETP Lett.* **22**, 274 (1975)].
- [2] M. B. Pogrebinskii, Mutual drag of carriers in a semiconductor-insulator-semiconductor system, *Fiz. Tekh. Poluprovodn.* **11**, 637 (1977) [*Sov. Phys. Semicond.* **11**, 372 (1977)].
- [3] J. M. Blatt, K. Böer, and W. Brandt, Bose-Einstein condensation of excitons, *Phys. Rev.* **126**, 1691 (1962).
- [4] M. Kellogg, J. P. Eisenstein, L. N. Pfeiffer, and K. W. West, Vanishing Hall resistance at high magnetic field in a double-layer two-dimensional electron system, *Phys. Rev. Lett.* **93**, 036801 (2004).
- [5] J.-J. Su and A. MacDonald, How to make a bilayer exciton condensate flow, *Nature Phys.* **4**, 799 (2008).
- [6] R. Wang, O. Erten, B. Wang, and D. Y. Xing, Prediction of a topological $p + ip$ excitonic insulator with parity anomaly, *Nature Commun.* **10**, 210 (2019).
- [7] D. Varsano, M. Palumbo, E. Molinari, and M. Rontani, A monolayer transition-metal dichalcogenide as a topological excitonic insulator, *Nature Nanotechnol.* **15**, 367 (2020).
- [8] E. Perfetto and G. Stefanucci, Floquet topological phase of nondriven p -wave nonequilibrium excitonic insulators, *Phys. Rev. Lett.* **125**, 106401 (2020).
- [9] Z. Sun and A. J. Millis, Topological charge pumping in excitonic insulators, *Phys. Rev. Lett.* **126**, 027601 (2021).
- [10] Z.-R. Liu, L.-H. Hu, C.-Z. Chen, B. Zhou, and D.-H. Xu, Topological excitonic corner states and nodal phase in bilayer quantum spin Hall insulators, *Phys. Rev. B* **103**, L201115 (2021).
- [11] H. D. Scammell, J. Ingham, T. Li, and O. P. Sushkov, Chiral excitonic order from twofold van Hove singularities in kagome metals, *Nat. Commun.* **14**, 605 (2023).
- [12] L. V. Keldysh and Y. V. Kopaev, Possible instability of the semimetallic state toward Coulomb interaction, *Sov. Phys. Solid State* **6**, 2219 (1965).

- [13] D. Jérôme, T. M. Rice, and W. Kohn, Excitonic insulator, *Phys. Rev.* **158**, 462 (1967).
- [14] B. Halperin and T. Rice, The excitonic state at the semiconductor-semimetal transition, *J. Phys. C: Solid State Phys.* **21**, 115 (1968).
- [15] R. Nandkishore and L. Levitov, Dynamical screening and excitonic instability in bilayer graphene, *Phys. Rev. Lett.* **104**, 156803 (2010).
- [16] K. W. Song, Y.-C. Liang, and S. Haas, Excitonic instabilities and insulating states in bilayer graphene, *Phys. Rev. B* **86**, 205418 (2012).
- [17] V. Apinyan and T. K. Kopeć, Excitonic gap formation and condensation in the bilayer graphene structure, *Phys. Scr.* **91**, 095801 (2016).
- [18] R. S. Akzyanov, A. O. Sboychakov, A. V. Rozhkov, A. L. Rakhmanov, and F. Nori, AA-stacked bilayer graphene in an applied electric field: Tunable antiferromagnetism and coexisting exciton order parameter, *Phys. Rev. B* **90**, 155415 (2014).
- [19] V. Apinyan and T. K. Kopeć, Antiferromagnetic ordering and excitonic pairing in AA-stacked bilayer graphene, *Phys. Rev. B* **104**, 075426 (2021).
- [20] H. Min, R. Bistritzer, J.-J. Su, and A. H. MacDonald, Room-temperature superfluidity in graphene bilayers, *Phys. Rev. B* **78**, 121401(R) (2008).
- [21] Y. E. Lozovik and A. A. Sokolik, Electron-hole pair condensation in a graphene bilayer, *JETP Lett.* **87**, 55 (2008).
- [22] C.-H. Zhang and Y. N. Joglekar, Excitonic condensation of massless fermions in graphene bilayers, *Phys. Rev. B* **77**, 233405 (2008).
- [23] M. Y. Kharitonov and K. B. Efetov, Electron screening and excitonic condensation in double-layer graphene systems, *Phys. Rev. B* **78**, 241401(R) (2008).
- [24] M. Y. Kharitonov and K. B. Efetov, Excitonic condensation in a double-layer graphene system, *Semicond. Sci. Technol.* **25**, 034004 (2010).
- [25] A. Perali, D. Neilson, and A. R. Hamilton, High-temperature superfluidity in double-bilayer graphene, *Phys. Rev. Lett.* **110**, 146803 (2013).
- [26] J.-J. Su and A. H. MacDonald, Spatially indirect exciton condensate phases in double bilayer graphene, *Phys. Rev. B* **95**, 045416 (2017).
- [27] D. K. Efimkin, G. W. Burg, E. Tutuc, and A. H. MacDonald, Tunneling and fluctuating electron-hole cooper pairs in double bilayer graphene, *Phys. Rev. B* **101**, 035413 (2020).
- [28] S. Conti, A. Perali, F. M. Peeters, and D. Neilson, Multicomponent screening and superfluidity in gapped electron-hole double bilayer graphene with realistic bands, *Phys. Rev. B* **99**, 144517 (2019).
- [29] G. W. Burg, N. Prasad, K. Kim, T. Taniguchi, K. Watanabe, A. H. MacDonald, L. F. Register, and E. Tutuc, Strongly enhanced tunneling at total charge neutrality in double-bilayer graphene-WSe₂ heterostructures, *Phys. Rev. Lett.* **120**, 177702 (2018).
- [30] L. Du, X. Li, W. Lou, G. Sullivan, K. Chang, J. Kono, and R.-R. Du, Evidence for a topological excitonic insulator in InAs/GaSb bilayers, *Nature Commun.* **8**, 1971 (2017).
- [31] X. Liu, K. Watanabe, T. Taniguchi, B. I. Halperin, and P. Kim, Quantum Hall drag of exciton condensate in graphene, *Nature Phys.* **13**, 746 (2017).
- [32] J. I. A. Li, T. Taniguchi, K. Watanabe, J. Hone, and C. R. Dean, Excitonic superfluid phase in double bilayer graphene, *Nature Phys.* **13**, 751 (2017).
- [33] J. I. A. Li, Q. Shi, Y. Zeng, K. Watanabe, T. Taniguchi, J. Hone, and C. R. Dean, Pairing states of composite fermions in double-layer graphene, *Nature Phys.* **15**, 898 (2019).
- [34] E. Tutuc, M. Shayegan, and D. A. Huse, Counterflow measurements in strongly correlated GaAs hole bilayers: Evidence for electron-hole pairing, *Phys. Rev. Lett.* **93**, 036802 (2004).
- [35] R. D. Wiersma, J. G. S. Lok, S. Kraus, W. Dietsche, K. von Klitzing, D. Schuh, M. Bichler, H.-P. Tranitz, and W. Wegscheider, Activated transport in the separate layers that form the $\nu_T = 1$ exciton condensate, *Phys. Rev. Lett.* **93**, 266805 (2004).
- [36] E. McCann and M. Koshino, The electronic properties of bilayer graphene, *Rep. Prog. Phys.* **76**, 056503 (2013).
- [37] E. McCann and V. I. Fal'ko, Landau-level degeneracy and quantum Hall effect in a graphite bilayer, *Phys. Rev. Lett.* **96**, 086805 (2006).
- [38] Y. Zhang, T.-T. Tang, C. Girit, Z. Hao, M. C. Martin, A. Zettl, M. F. Crommie, Y. R. Shen, and F. Wang, Direct observation of a widely tunable bandgap in bilayer graphene, *Nature (London)* **459**, 820 (2009).
- [39] H. D. Scammell and O. P. Sushkov, Dynamical screening and excitonic bound states in biased bilayer graphene, *Phys. Rev. B* **107**, 085104 (2023).
- [40] V. Berestetskii, E. Lifshitz, and L. Pitaevskii, *Quantum Electrodynamics: Vol. 4*, Course of theoretical physics (Elsevier Science, Amsterdam, 1982).
- [41] M. J. Yang, C. H. Yang, B. R. Bennett, and B. V. Shanabrook, Evidence of a hybridization gap in "semimetallic" InAs/GaSb systems, *Phys. Rev. Lett.* **78**, 4613 (1997).
- [42] S. Saberi-Pouya, S. Conti, A. Perali, A. F. Croxall, A. R. Hamilton, F. M. Peeters, and D. Neilson, Experimental conditions for the observation of electron-hole superfluidity in GaAs heterostructures, *Phys. Rev. B* **101**, 140501(R) (2020).
- [43] Z. Bi and L. Fu, Excitonic density wave and spin-valley superfluid in bilayer transition metal dichalcogenide, *Nature Commun.* **12**, 642 (2021).
- [44] B. Roy and I. F. Herbut, Unconventional superconductivity on honeycomb lattice: Theory of Kekule order parameter, *Phys. Rev. B* **82**, 035429 (2010).
- [45] T. Li, J. Ingham, and H. D. Scammell, Artificial graphene: Unconventional superconductivity in a honeycomb superlattice, *Phys. Rev. Res.* **2**, 043155 (2020).
- [46] T. Li, M. Geier, J. Ingham, and H. D. Scammell, Higher-order topological superconductivity from repulsive interactions in kagome and honeycomb systems, *2D Mater.* **9**, 015031 (2022).
- [47] R. T. Weitz, M. T. Allen, B. E. Feldman, J. Martin, and A. Yacoby, Broken-symmetry states in doubly gated suspended bilayer graphene, *Science* **330**, 812 (2010).
- [48] F. Freitag, J. Trbovic, M. Weiss, and C. Schönnenberger, Spontaneously gapped ground state in suspended bilayer graphene, *Phys. Rev. Lett.* **108**, 076602 (2012).
- [49] L. Ju, L. Wang, T. Cao, T. Taniguchi, K. Watanabe, S. G. Louie, F. Rana, J. Park, J. Hone, F. Wang, and P. L. McEuen, Tunable excitons in bilayer graphene, *Science* **358**, 907 (2017).